Catalyst Effects in Heterogeneous Nucleation of Acicular Ferrite

Ø. GRONG, A.O. KLUKEN, H.K. NYLUND, A.L. DONS, and J. HJELEN

The present investigation is concerned with basic studies of the mechanisms of acicular ferrite (AF) formation in low-alloy steel weld metal. It is confirmed experimentally that different types of orientation relationships exist between AF and specific cubic inclusion constituent phases (*i.e.*, γ-Al_2O_3, $MnOAl_2O_3$, and TiN). Since the majority of these falls within the Bain orientation region, it is concluded that the associated reduction of the energy barrier to nucleation is the primary cause for the ferrite nucleus to develop orientation relationships with both the substrate and the austenite. Theoretical calculations show that about 12 pct of the inclusions will contain a cubic phase that lies within the Bain region purely by chance if they are randomly orientated in space. This intrinsic density of heterogeneous nucleation sites is sufficiently high to promote the formation of fine, interlocking AF laths in the weld metal during the γ-to-α transformation.

I. INTRODUCTION

ASPECTS of acicular ferrite (AF) formation in low-alloy steel weld metals have been extensively reported and investigated in the literature.[1–7] It is well established that this microconstituent nucleates at indigenous nonmetallic inclusions in the transformation temperature range between Widmannstätten ferrite and lower bainite.[8,9] Based on the electron backscattering pattern (EBSP) technique, Kluken *et al.*[10] have shown that the AF plates exhibit an orientation relationship with both the austenite and the prior delta ferrite columnar grains in which they grow. The observed orientation relationship lies within the Bain orientation region and can be described by three texture components, *i.e.*, a ⟨100⟩ component and two complementary ⟨111⟩ components. Each of these texture components is orientated approximately parallel with the original cell/dendrite growth direction. Moreover, measurements of the spatial misorientation between neighboring plates confirm that the morphology of AF in low-alloy steel weld metals bears a close resemblance to upper bainite.[10] This suggests that growth of the AF plates occurs either by a ledge mechanism or by a pure shear transformation, similar to that documented for bainite in wrought steel.

However, from the literature reviewed, it is obvious that conflicting views are held about the major controlling nucleation mechanism.[5–12] In particular, it is essential to clarify whether the AF plates also adopt rational orientation relationships with the substrate in order to minimize the energy barrier to nucleation. This, in turn, could explain why certain types of inclusions (particularly those containing Al and Ti) appear to be much more favorable nucleation sites for AF than others.[5,7] At present, a complete understanding of the development of the AF microstructure in low-alloy steel weld metals is lacking.

Ø. GRONG and J. HJELEN, Professors, are with the Department of Metallurgy, University of Trondheim, The Norwegian Institute of Technology, N-7034 Trondheim, Norway. A.O. KLUKEN, Senior Research Metallurgist, is with Hydro Aluminium, Research Centre-Karmöy, N-4265 Håvik, Norway. H.K. NYLUND, Ph.D. Student, is with SINTEF-Materials Technology, N-0314 Oslo, Norway. A.L. DONS, Senior Research Metallurgist, is with SINTEF-Materials Technology, N-7034 Trondheim, Norway.

Manuscript submitted October 18, 1993.

II. EXPERIMENTAL DETAILS

A. *Materials*

For this investigation, a 1.6-mm-diameter tubular electrode wire was selected. Bead deposition was carried out with a mechanized unit for submerged arc (SA) welding under a commercial basic flux, using the same welding procedure as described in Reference 13. Details of the weld metal inclusion characteristics and solidification microstructure have been reported elsewhere.[13,14] Table I contains a summary of weld chemical composition and operational conditions.

B. *Preparation of Thin Foils*

The thin foils for the transmission electron microscope (TEM) analysis were taken from the area close to the weld centerline. Specifically, the preparation procedure involved mechanical grinding down to about 0.1 mm, with subsequent thinning in an automatic jet-polishing apparatus (operating at +20 °C and 26 V), using a 95 vol pct 2 butoxyethanol −5 vol pct perchloric acid solution as electrolyte.

C. *Transmission Electron Microscopy*

The thin foils were examined in a PHILIPS* CM 30 transmission electron microscope equipped with an EDAX** energy dispersive spectrometer (EDS). The various inclusion constituent phases were analyzed and identified from selected area diffraction patterns and X-ray microanalysis of particles located within the foils. The former technique was also employed for measurements of orientation relationships between the inclusions and contiguous acicular ferrite plates. All of these are based on single observations.

*PHILIPS is a trademark of Philips Electronic Instruments Corp., Mahwah, NJ.

**EDAX is a trademark of Philips Electronic Instruments, Inc., Mahwah, NJ.

Table I. Summary of Weld-Metal Chemical Composition and Operational Conditions

Element (Wt Pct)	Pct C	Pct O	Pct Si	Pct Mn	Pct P	Pct S	Pct Al (tot)	Pct Al (sol)	Pct Ti
Weld 3*	0.10	0.035	0.69	1.88	0.012	0.010	0.028	0.003	0.063

*Operational conditions: 450 *A*-30 *V*-2.6 mm/s; E = 5.2 kJ/mm.
Same numbering as in Refs. 13 and 14.

III. RESULTS

The TEM examination revealed the existence of three different constituent phases, *i.e.*, γ-Al_2O_3, $MnOAl_2O_3$, and TiN. Details of lattice parameters and crystal structures are given in Table II.

A. γ-Al_2O_3 Inclusions

In the following, conjugate planes between the inclusions and the ferrite are indicated by ordinary parentheses, while square brackets denote parallel zone axes. Moreover, the subscript α refers to matrix reflection spots in the diffraction pattern.

Figure 1(a) shows a bright-field image of a γ-Al_2O_3 inclusion embedded in a matrix of AF. A closer inspection of the diffraction patterns in Figure 1(b) reveals that the 200-type particle reflections are approximately aligned in the direction of the 110-type matrix reflections. If the small angle distortion between the incident beam and the zone axes is neglected (which gives rise to an unsymmetrical diffraction pattern), we obtain the following orientation relationship between γ-Al_2O_3 and AF:

$$(100)_{\gamma\text{-}Al_2O_3} \sim // (011)_{\alpha\text{-}Fe}$$

$$[01\bar{1}]_{\gamma\text{-}Al_2O_3} \sim // [5\bar{3}3]_{\alpha\text{-}Fe}$$

B. $MnOAl_2O_3$ Inclusions

In this case, two different orientation relationships can be detected. Referring to Figure 2, a parallelism exists between the 200-type particle reflections and the 110-type matrix reflections, but the exact orientation relationship cannot be established because of overlap in the matrix reflections from different zone axes. Another relationship is shown in Figure 3, where the 110-type particle reflections are aligned in the direction of the 200-type matrix reflections. Since the zone axes here coincide with the $(0\bar{1}1)$ and (001) plane normals,* we obtain

$$(011)_{MnOAl_2O_3} // (010)_{\alpha\text{-}Fe}$$

$$[0\bar{1}1]_{MnOAl_2O_3} // [001]_{\alpha\text{-}Fe}$$

*The matrix zone axis was determined from a second picture, using a larger selected area diffraction (SAD) aperture.

Table II. Identified Constituent Phases in Weld-Metal Inclusions

Phase	Crystal Structure	Lattice Parameter (Å)
γ-Al_2O_3	distorted spinel	7.85
$MnOAl_2O_3$	spinel	8.27
TiN	NaCl (fcc)	4.25

Fcc: face-centered cubic.

C. TiN Inclusions

As shown in Figure 4, a parallelism exists between the 110-type particle reflections and the 200-type matrix reflections. At the same time, a good lattice matching is observed in directions that lie normal to these reflections in the diffraction image. Since the two zone axes in this case are parallel, we get

$$(\bar{1}10)_{TiN} // (100)_{\alpha\text{-}Fe}$$

$$(112)_{TiN} // (011)_{\alpha\text{-}Fe}$$

$$[11\bar{1}]_{TiN} // [0\bar{1}1]_{\alpha\text{-}Fe}$$

In addition, two other variants are shown in Figures 5 and 6. These can approximately be described as

$$(10\bar{1})_{TiN} // (\bar{1}03)_{\alpha\text{-}Fe}$$

$$(320)_{TiN} // (112)_{\alpha\text{-}Fe}$$

$$[2\bar{3}2]_{TiN} // [3\bar{5}1]_{\alpha\text{-}Fe}$$

and

$$(\bar{1}01)_{TiN} // (\bar{1}33)_{\alpha\text{-}Fe}$$
$$(221)_{TiN} // (200)_{\alpha\text{-}Fe}$$

Table III contains a summary of the different orientation relationships observed in the present investigation.

IV. DISCUSSION

The observed orientation relationships can be interpreted in different ways. Previous investigations have shown that small, incoherent precipitates in steel (1 to 5 nm) can rotate into coherence with the austenite during heat treatment and thus bear an orientation relationship with the matrix.[15] However, considering the fact that the rotation rate quickly diminishes for larger particles, this possibility can be excluded when it is recognized that the typical size of a weld metal inclusion is between 0.1 and 1 μm.[13] It is, therefore, reasonable to assume that the associated reduction of the energy barrier to nucleation is the primary cause for the ferrite nucleus to develop orientation relationships with both the substrate and the austenite. In the following, the probability of this happening will be examined more in detail.

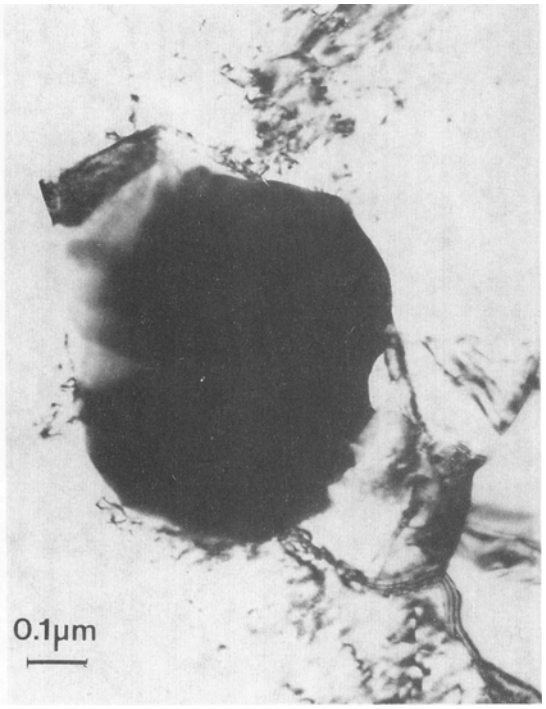

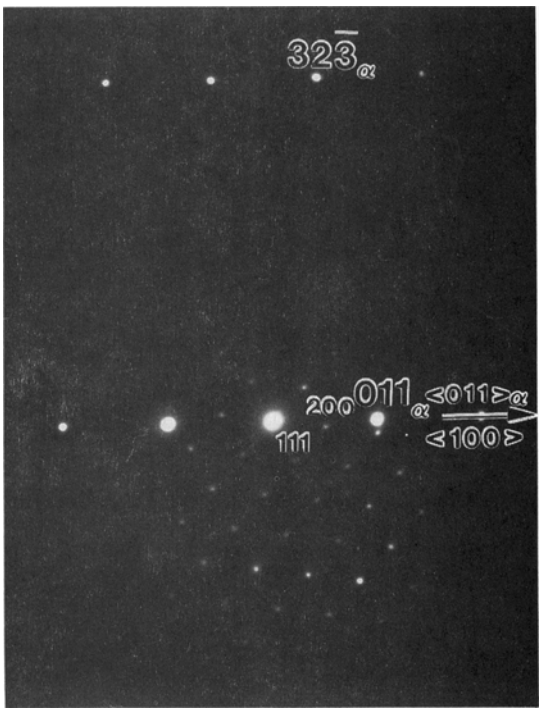

(*a*) (*b*)

Fig. 1—Observed orientation relationship between γ-Al_2O_3 and AF: (*a*) bright-field image of inclusion and surrounding ferrite matrix and (*b*) resulting diffraction patterns.

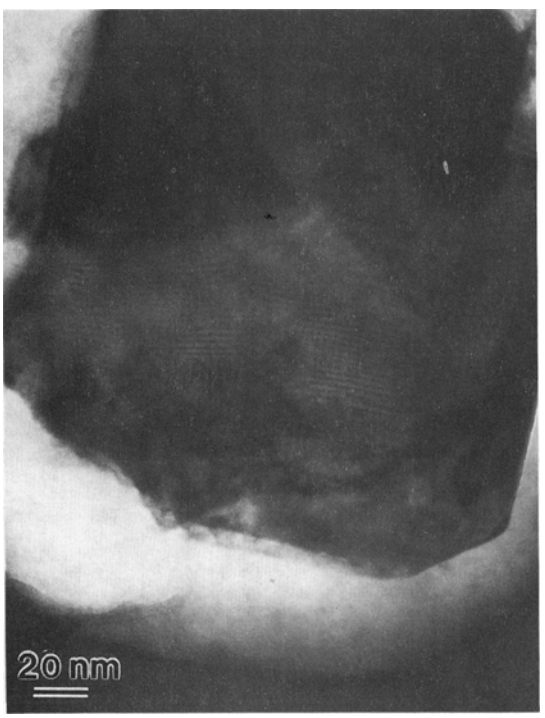

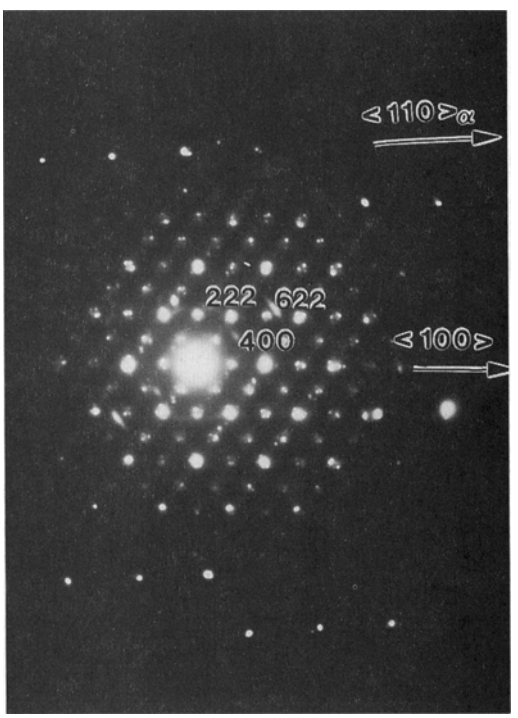

(*a*) (*b*)

Fig. 2—Observed orientation relationship between $MnOAl_2O_3$ and AF (first variant): (*a*) bright-field image of inclusion and surrounding ferrite matrix and (*b*) resulting diffraction patterns.

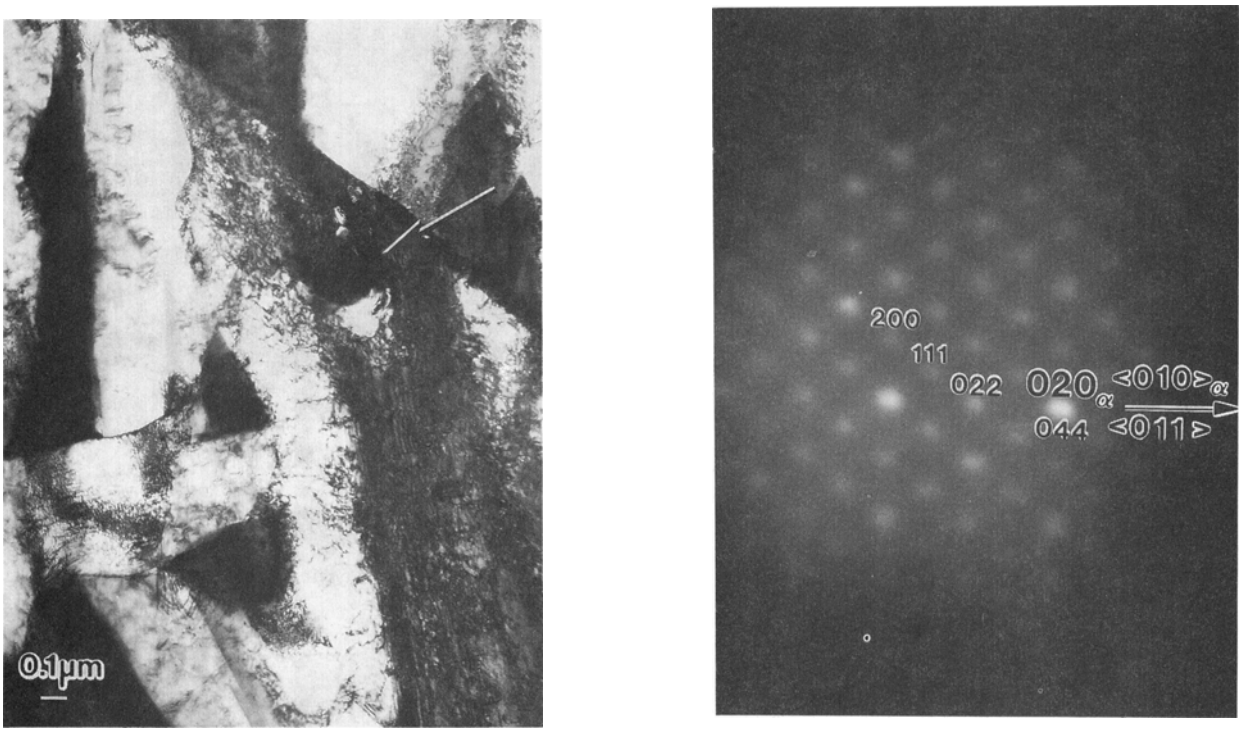

(*a*) (*b*)

Fig. 3—Observed orientation relationship between $MnOAl_2O_3$ and AF (second variant): (*a*) bright-field image of inclusion and surrounding ferrite matrix and (*b*) resulting diffraction patterns.

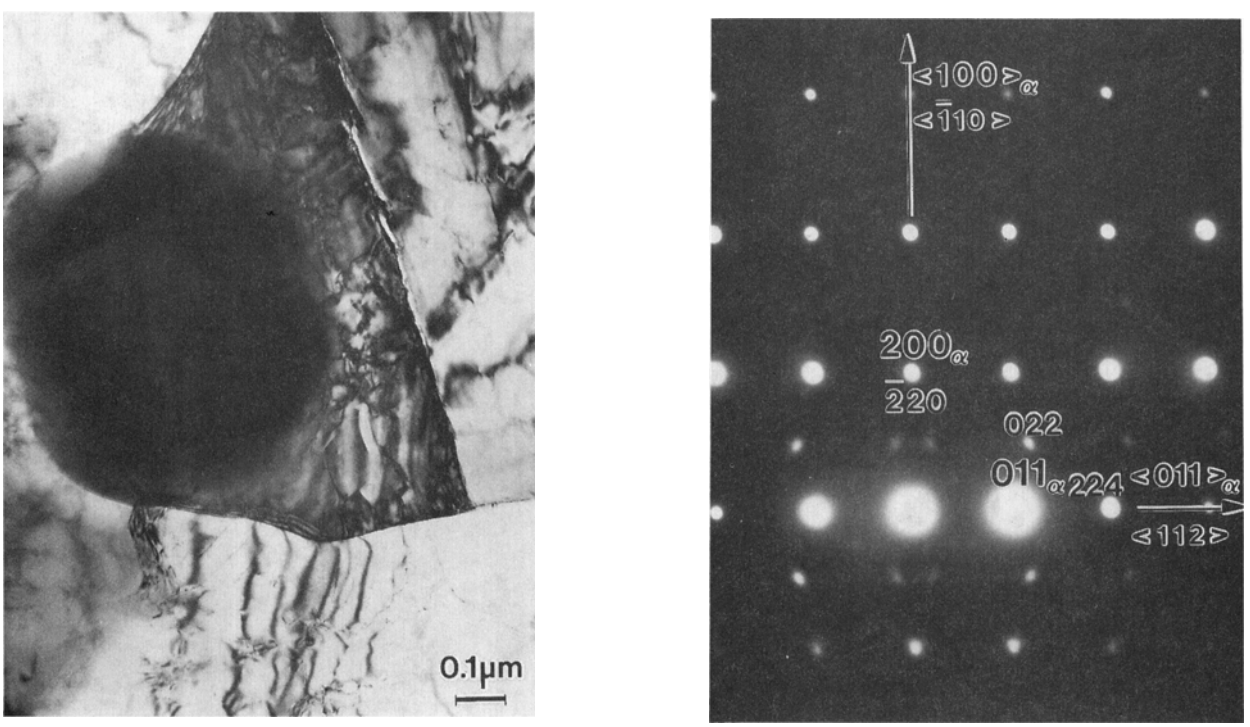

(*a*) (*b*)

Fig. 4—Observed orientation relationship between TiN and AF (first variant): (*a*) bright-field image of inclusion and surrounding ferrite matrix and (*b*) resulting diffraction patterns.

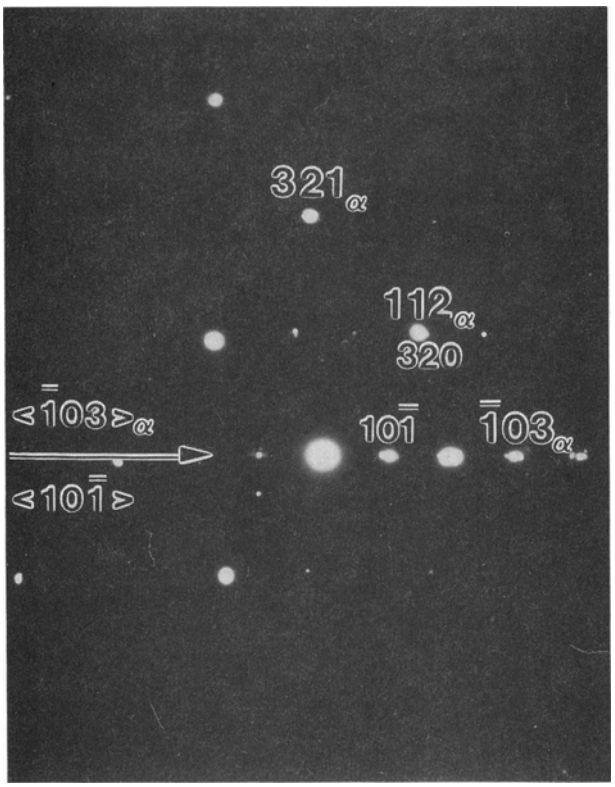

Fig. 5—Observed orientation relationship between TiN and AF (second variant).

A. *Constituent Elements and Phases in Inclusions*

Nonmetallic inclusions commonly found in steel weld metals are almost always seen to be heterogeneous in nature both with respect to chemistry (multiphase particles), shape (angular or spherical particles), and crystallographic properties because of the complex alloying systems involved.[5,13]

It can be inferred from the deoxidation model of Kluken and Grong[13] that the chemical composition of the inclusion oxide core is directly related to the [Δ pct Al]/[pct O] ratio in the weld metal, where [Δ pct Al] is the measured difference between total and acid soluble aluminum, and [pct O] is the analytical weld metal oxygen content. Referring to Figure 7, the fraction of $MnOAl_2O_3$ and γ-Al_2O_3 in the inclusions is seen to increase with increasing [Δ pct Al]/[pct O] ratios until the stoichiometric composition for precipitation of aluminum oxide is reached at 1.13. At higher ratios, the deoxidation product will be pure Al_2O_3, since aluminum is present in an overstoichiometric amount with respect to oxygen. When titanium is added to the weld metal, titanium oxide (probably in the form of Ti_2O_3) may also enter the reaction product. At the same time, both TiN and α-MnS tend to form on the surface of the inclusions. Precipitation of these phases occurs after the completion of the weld-metal deoxidation, probably during solidification, where the reactions are favored by solute enrichment in the interdendritic liquid.[13]

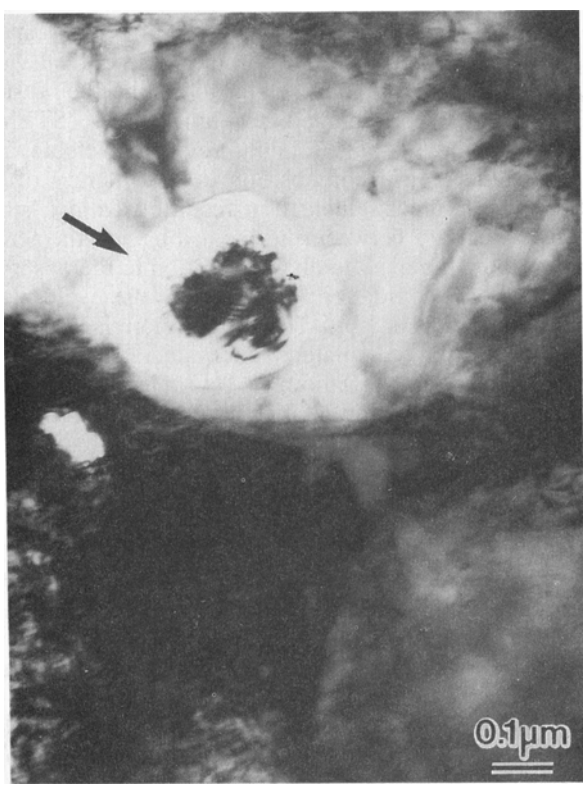

(*a*)

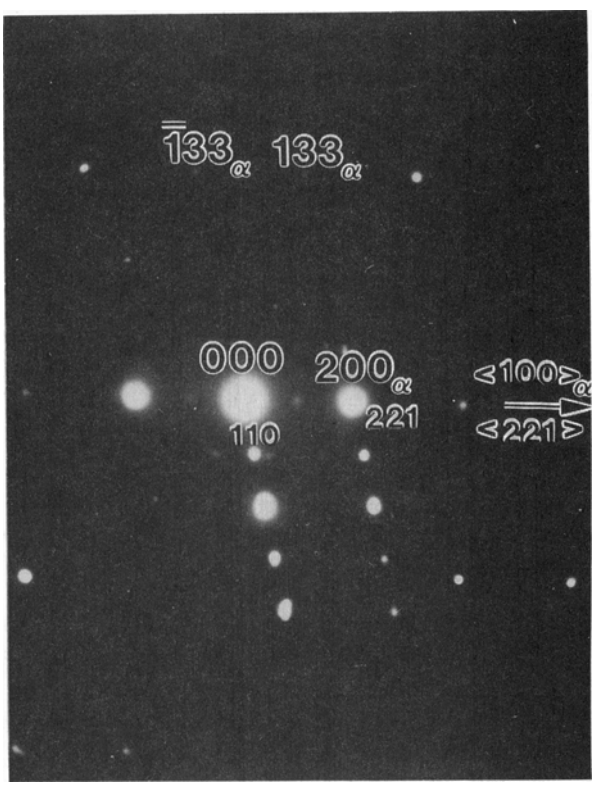

(*b*)

Fig. 6—Observed orientation relationship between TiN and AF (third variant): (*a*) bright-field image of inclusion and surrounding ferrite matrix and (*b*) resulting diffraction patterns.

Table III. Observed Orientation Relationships between AF and Different Inclusion Constituent Phases in Experimental Weld

Substrate (s)	Orientation Relationship		Interplanar Spacing	
	Type/Variant	Number	Plane Combinations	Ratio*
γ-Al_2O_3 (distorted spinel)	$(100)_s \sim // (011)_{\alpha\text{-Fe}}$	1	$\{011\}_{\alpha\text{-Fe}}$ and $\{400\}_s$	1.02
	$[01\bar{1}]_s \sim // [53\bar{3}]_{\alpha\text{-Fe}}$			
$MnOAl_2O_3$ (spinel)	$(200)_s \sim // (110)_{\alpha\text{-Fe}}$	2	$\{110\}_{\alpha\text{-Fe}}$ and $\{400\}_s$	0.99
	$(011)_s // (010)_{\alpha\text{-Fe}}$	3	$\{200\}_{\alpha\text{-Fe}}$ and $\{440\}_s$	0.99
	$[0\bar{1}1]_s // [001]_{\alpha\text{-Fe}}$			
TiN (NaCl)	$(\bar{1}10)_s // (100)_{\alpha\text{-Fe}}$	4	$\{200\}_{\alpha\text{-Fe}}$ and $\{220\}_s$	0.97
	$(112)_s // (011)_{\alpha\text{-Fe}}$		$\{011\}_{\alpha\text{-Fe}}$ and $\{112\}_s$	1.17
	$[11\bar{1}]_s // [0\bar{1}1]_{\alpha\text{-Fe}}$			
	$(10\bar{1})_s // (\bar{1}03)_{\alpha\text{-Fe}}$	5	$\{310\}_{\alpha\text{-Fe}}$ and $\{330\}_s$	0.91
	$(320)_s // (112)_{\alpha\text{-Fe}}$		$\{112\}_{\alpha\text{-Fe}}$ and $\{320\}_s$	0.99
	$[2\bar{3}2]_s // [3\bar{5}1]_{\alpha\text{-Fe}}$			
	$(\bar{1}01)_s // (\bar{1}33)_{\alpha\text{-Fe}}$	6	$\{133\}_{\alpha\text{-Fe}}$ and $\{550\}_s$	1.10
	$(221)_s // (200)_{\alpha\text{-Fe}}$		$\{200\}_{\alpha\text{-Fe}}$ and $\{221\}_s$	1.01

*Defined as $d(hkl)_{\alpha\text{-Fe}}/d(hkl)_s$.

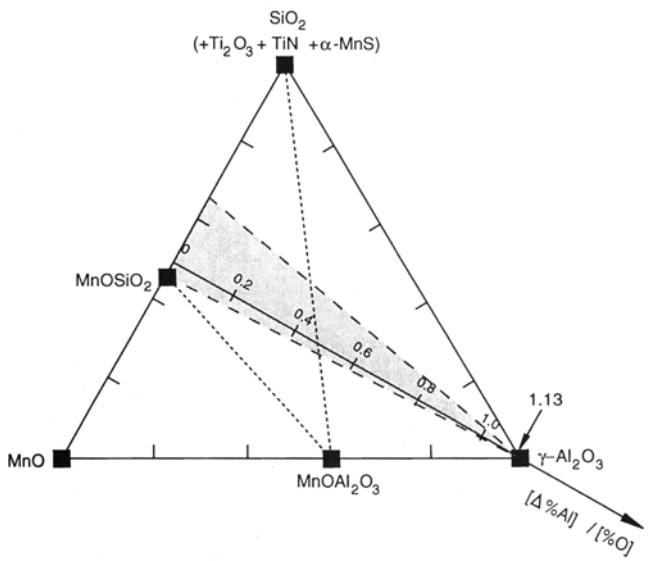

Fig. 7—Coexisting phases in inclusions at different weld-metal aluminum-to-oxygen ratios. Shaded region indicates the approximate composition range for the oxide phase. The diagram is constructed on the basis of the model of Kluken and Grong[13] and relevant literature data.

B. *Catalyst Effects in Heterogeneous Nucleation*

As mentioned in Section I, there is considerable circumstantial evidence available in the scientific literature that intragranular nucleation of AF is preferentially associated with specific types of nonmetallic inclusions (*i.e.*, γ-Al_2O_3, $MnOAl_2O_3$, and TiN).[5,6,8,16–24] Different mechanisms have been proposed over the years to explain these phenomena, including:[5,7,8,18,21]

(1) nucleation resulting from a small lattice disregistry between the inclusions and the ferrite;
(2) nucleation in the vicinity of inclusions caused by local compositional inhomogeneity in the steel matrix; and
(3) nucleation in the vicinity of inclusions resulting from favorable strain or dislocation arrays due to differences in the thermal contraction between the particles and the matrix.

Because of the complexity of the weld-metal inclusions, and the experimental difficulties involved in performing controlled (*in situ*) measurements, it cannot be stated with certainty which of these three mechanisms that are operative during the AF transformation. However, based on simple theoretical calculations, it can be argued that the contribution from the elastic strain fields around the particles due to differential contraction effects probably is too insignificant to influence the free energy of transformation and that the resulting punching-stress at the particle/matrix interface is well below the critical value required to generate new dislocations in the austenite.[4,25] Moreover, detailed scanning TEM (STEM)/EDS microanalyses have failed to reveal detectable variations in the matrix composition in the vicinity of the inclusions.[2] Hence, nucleation resulting from a small lattice disregistry between the inclusions and the ferrite appears to be the most likely explanation to the observed influence of deoxidation practice on the weld-metal transformation behavior. This conclusion is also supported by the calculated interplanar spacings in Table III, showing that both γ-Al_2O_3, $MnOAl_2O_3$, and TiN provide a good lattice matching with the ferrite in, at least, one crystallographic direction for all six orientations indicated.

C. *Conditions for Ferrite Formation at Inclusions*

From a theoretical standpoint, the development of a faceted ferrite nucleus that exhibits a rational orientation relationship with both the austenite and the inclusions would require that the substrate and the austenite have similar crystal structures and identical lattice orientations.[26] The catalyst particles must, therefore, be cubic and bear an orientation relationship with the austenite that lies within the Bain region. In addition, they should be faceted and exhibit an atomic arrangement that matches that of the ferrite across the interface. Although the latter condition is clearly satisfied under the prevailing circumstances, the former requirement cannot

generally be met because the weld-metal inclusions form in the liquid state prior to the solidification process.[27] Nevertheless, even if the orientation of the inclusions were perfectly random, it is apparent that orientation relations within the Bain region would be observed purely by chance. In view of the high symmetry of the cubic system, the probability of this happening must be calculated. An approximative estimate is given below for single-phase cubic inclusions, based on the method described by Ryder *et al.*[28]

Figure 8 contains a standard stereographic projection of the austenite crystal, showing the $\langle 100 \rangle_{\gamma\text{-Fe}}$ poles (squares) and the $\langle 110 \rangle_{\gamma\text{-Fe}}$ poles (dots). The Bain orientation region is represented by small circles with a radius of 11 deg centered on the $\langle 100 \rangle_{\gamma\text{-Fe}}$ and the $\langle 110 \rangle_{\gamma\text{-Fe}}$ poles.[28] The austenite/inclusion (i) orientation relationship is within the orientation region derived from the Bain correspondence, if one $\langle 100 \rangle_i$ pole lies within a $\langle 100 \rangle_{\gamma\text{-Fe}}$ region and the other two $\langle 100 \rangle_i$ poles lie within $\langle 110 \rangle_{\gamma\text{-Fe}}$ regions. Assuming a random inclusion orientation, the probability P_1 that a given $\langle 100 \rangle_i$ pole lies within a given $\langle 100 \rangle_{\gamma\text{-Fe}}$ region is $\omega/4\pi$, where ω is the solid angle enclosed by one $\langle 100 \rangle_{\gamma\text{-Fe}}$ region (equal to $2\pi(1 - \cos 11 \text{ deg}) = 0.115$). Since there are three $\langle 100 \rangle_i$ directions and six $\langle 100 \rangle_{\gamma\text{-Fe}}$ regions, the probability that at least one $\langle 100 \rangle_i$ pole lies within a $\langle 100 \rangle_{\gamma\text{-Fe}}$ region is equal to

$$P_1 = 3 \times 6 \times \frac{\omega}{4\pi} = 0.165$$

Imagine, now, that the inclusion lattice is rotated through 360 deg about the $\langle 100 \rangle_i$ axis, which lies within a $\langle 100 \rangle_{\gamma\text{-Fe}}$ region. The other two $\langle 100 \rangle_i$ poles will then lie within $\langle 110 \rangle_{\gamma\text{-Fe}}$ regions for at the most 4 × 22 deg = 88 deg of this rotation, since the diameter of the $\langle 100 \rangle_{\gamma\text{-Fe}}$ regions is 22 deg. Hence, the probability P_2 that if one $\langle 100 \rangle_i$ pole lies within a $\langle 100 \rangle_{\gamma\text{-Fe}}$ region, the other two will lie within $\langle 110 \rangle_{\gamma\text{-Fe}}$ regions is given in the upper limit by

$$P_2 \leq \frac{88}{360} = 0.244$$

The total probability that a given orientation relationship lies within the Bain region purely by change is thus

$$P \leq P_1 \times P_2 = 0.165 \times 0.244 = 0.04$$

Therefore, assuming random orientation, about 4 pct of the weld-metal inclusions would lie within the Bain region purely by chance if they were single-phase cubic crystals. In practice, however, inclusions commonly found in low-alloy steel weld metals are of a very heterogeneous chemical and crystalline nature. As shown in Figure 7, a typical inclusion may contain up to six different constituent phases, including the three cubic phases γ-Al_2O_3, $MnOAl_2O_3$, and TiN. This implies that at least 12 pct of the inclusions may contain a cubic phase that lies within the Bain orientation region.

The measured orientation relationships in Table III support the preceding interpretation. Referring to the standard stereographic projections in Figure 9, a very high proportion of the ferrite/inclusion orientations falls within the Bain region. In addition, two other variants (*i.e.*, numbers 5 and 6) are indicated for TiN that do not meet this requirement. They are therefore regarded as spurious (in the sense that the measured diffraction patterns do not stem from a catalyst nucleation event) and should be ignored. Hence, the observed orientation relationships between AF and specific inclusion constituent phases are not fully reproducible in the true meaning of the word, since only those combinations that satisfy the inherent crystallography of the AF microstructure are acceptable.

Based on this probability analysis, it is possible to estimate an upper limit for the volume of a typical plate of AF under conditions applicable to steel welding. In general, Ti-Al deoxidized steel weld metals contain between 2×10^7 and 8×10^7 inclusions/mm^3.[13] If we take $N_v = 4 \times 10^7$ mm^{-3} as a reasonable average and then assume random orientation and only one nucleation event per inclusion, the following upper limit for the AF plate volume is obtained:

$$V_{AF} \leq \frac{1}{3 \times P \times N_v}$$

$$= \frac{1}{3 \times 0.04 \times (4 \times 10^7)} \text{ mm}^3 \approx 2 \times 10^{-7} \text{ mm}^3$$

The volume V_{AF} corresponds to an AF plate that has the shape of a square lath with a side of 10 μm and thickness of 2 μm. Although this estimate is in reasonable agreement with experimental observations,[27] the prediction is conservative in the sense that it assumes only one nucleation event per inclusion. In practice, an oxide inclusion that is orientated within the Bain region has the capability of nucleating several AF plates, as shown by

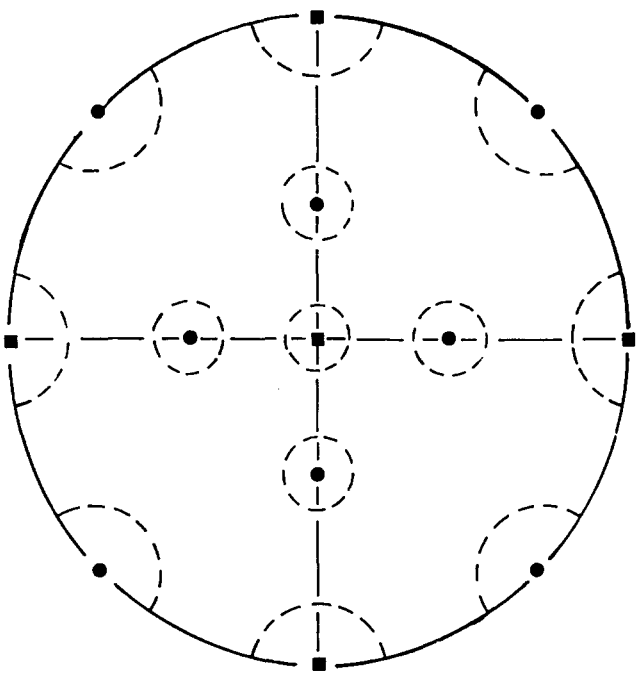

Fig. 8—Stereographic projection of Bain regions represented by 11-deg circles, round $\langle 100 \rangle_{\gamma\text{-Fe}}$ poles (squares), and $\langle 110 \rangle_{\gamma\text{-Fe}}$ poles (dots) of the austenite lattice (after Ryder *et al.*[28]).

the scanning electron microscope (SEM) micrograph in Figure 10. In addition, the AF plates may nucleate autocatalytically at α_{Fe}/γ_{Fe} boundaries, a process that also is referred to as sympathetic nucleation in the literature.[2,5,27,29] At present, it is not clear to what extent autocatalytic nucleation plays a role in the development of the AF microstructure.

D. *Practical Implications*

Simple verification on the basis of classic nucleation theory shows that the associated reduction of the energy barrier to nucleation, $\Delta G^*_{het.}$, is the primary cause for the ferrite nucleus to develop orientation relationships with both the substrate and the austenite.[26,30] It is evident from the data in Table III that both γ-Al_2O_3, $MnOAl_2O_3$, and TiN reveal a good lattice matching with the ferrite phase in one crystallographic direction. In addition, nucleation of AF at TiN offers the advantage of partial lattice coherence in a second (independent) direction, which further may contribute to a reduction of $\Delta G^*_{het.}$ through a minimization of the interfacial energy between the two phases. This makes TiN an extremely efficient nucleant for AF.

Microstructure data available for SA steel-weld deposits clearly support the above findings that nucleation of AF occurs preferentially at inclusions that contain aluminum or titanium. As shown in Figure 11, a high volume fraction of AF is always achieved when sufficient amounts of titanium are added either through the filler wire or the flux, irrespectively of the aluminum and oxygen concentrations. This occurs in spite of a reduction in the columnar austenite grain size[14] and is in sharp contrast to welds produced with welding consumables containing low levels of titanium, where the AF content drops rapidly with decreasing [Δ pct Al]/[pct O] ratios due to the presence of lower fractions of γ-Al_2O_3 and $MnOAl_2O_3$ in the inclusions (Figure 7). Similar observations have also been made by other investigators.[5,17–20,22,23]

It should be noted that the weld-metal transformation behavior, in practice, depends on complex interactions between a number of important variables, including alloying and deoxidation practice, the solidification microstructure, the prior austenite grain size, and the weld thermal cycle.[5,6,8] This means that the presence of γ-Al_2O_3, $MnOAl_2O_3$, or TiN at the surface of the inclusions is not a sufficient criterion for formation of AF in steel weld metals.

Finally, an interesting observation from the data in Table III is that nucleation of acicular ferrite at inclusions is always associated with low-index planes of the {100} or the {110} type, which indicates a faceted growth morphology of the inclusions. Faceted growth may occur as a result of anisotropy in the growth rates between high-index and low-index crystallographic planes and can in the extreme case lead to a morphology of the type shown in Figure 12. Consequently, the development of faceted inclusions in the liquid steel during deoxidation appears to be an intrinsic feature of low-alloy steel weld metals.

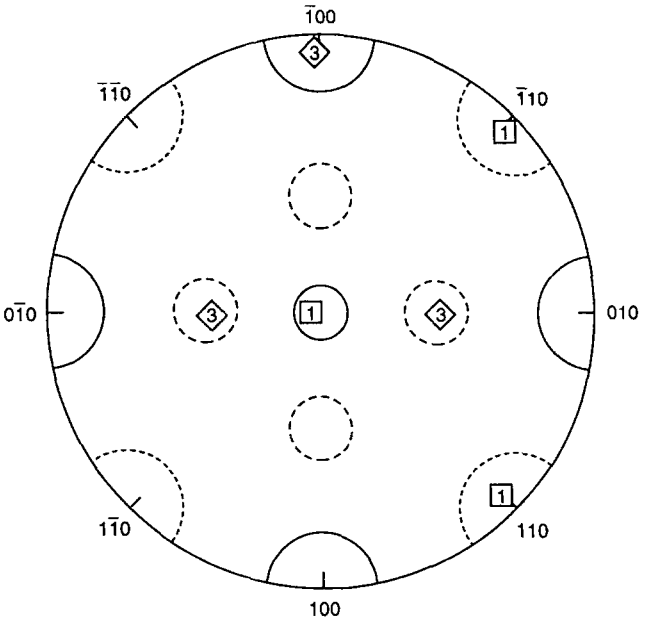

Fig. 9—Standard (100) stereographic projections of the orientation relationships listed in Table III: (*a*) numbers (1) and (3) and (*b*) numbers (4), (5), and (6). The Bain orientation region is indicated by the 11-deg circles in the graphs. See Fig. 8 for details.

V. CONCLUSIONS

The main conclusions that can be drawn from this investigation are as follows:

1. It is confirmed experimentally that different types of orientation relationships exist between AF and specific cubic inclusion constituent phases (*i.e.*, γ-Al_2O_3, $MnOAl_2O_3$, and TiN). The majority of these orientation relationships fall within the Bain orientation region.

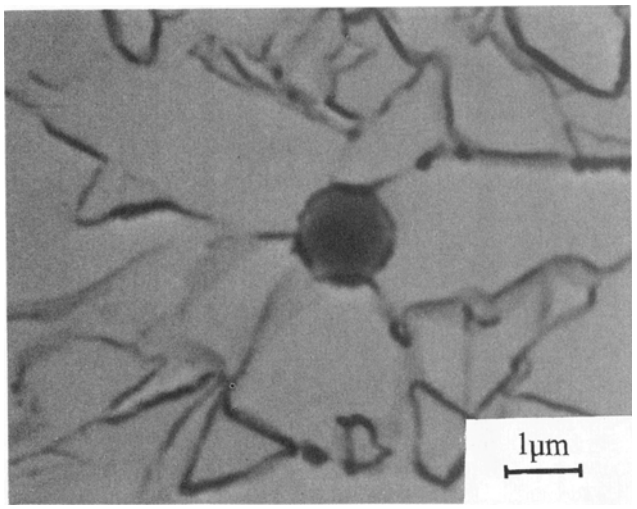

Fig. 10—SEM micrograph of a carbon extraction replica showing evidence of multiple nucleation of AF at a weld-metal inclusion.

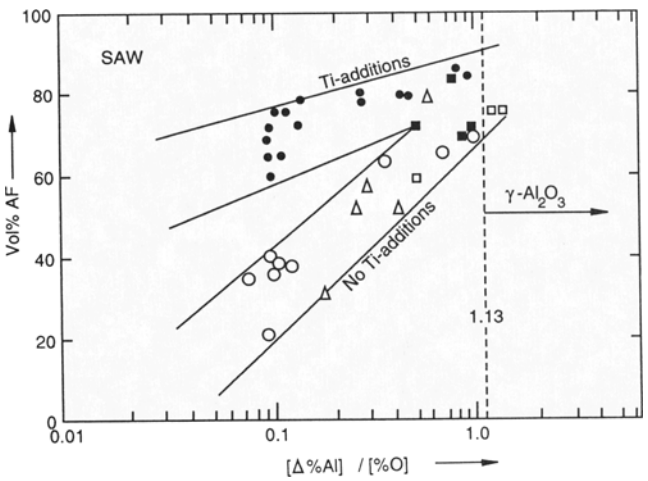

Fig. 11—Effect of deoxidation practice (inclusion chemistry) on the AF transformation in low-alloy steel weld metals (data from Refs. 20, 31, and 32).

2. Since the weld-metal inclusions form in the molten pool before solidification, they are presumably randomly orientated with respect to the parent austenite phase. Under such conditions, theoretical calculations show that at least 12 pct of the inclusions will contain a cubic phase that lies within the Bain orientation region purely by chance.
3. Assuming random particle orientation and only one nucleation event per inclusion, an upper limit for the AF plate volume of about 2×10^{-7} mm^3 has been calculated. This value corresponds to an AF plate that has the shape of a square lath with a side of 10 μm and a thickness of 2 μm.
4. The indications are that the associated reduction of the energy barrier to nucleation is the primary cause for the ferrite nucleus to develop orientation relationships with both the inclusions and the austenite. A qualitative ranking of the different constituent phases indicates that their nucleation potency with respect to

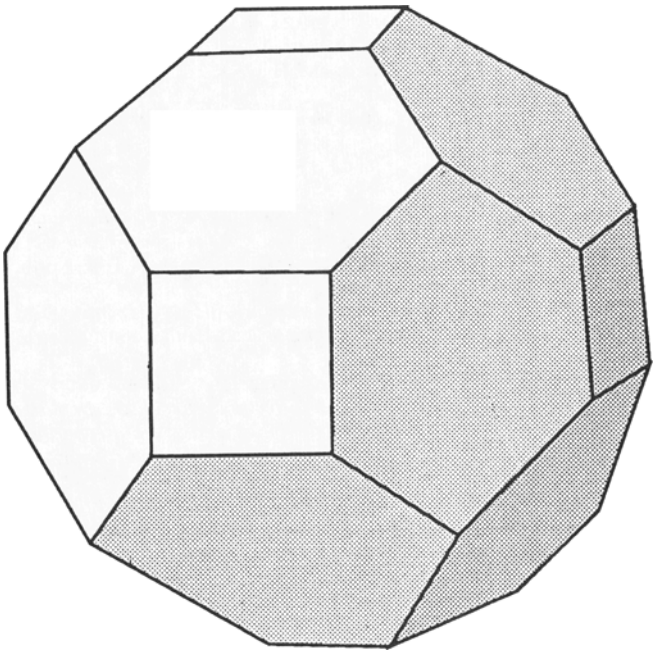

Fig. 12—Example of a faceted crystal delimited by {100} and {110} planes (schematic).

AF increases in the order γ-Al_2O_3, $MnOAl_2O_3$, and TiN. The effectiveness of the TiN particles can be attributed to a small lattice disregistry between the substrate and the ferrite nucleus, which reduces the energy barrier to nucleation at these sites through a minimization of the interfacial energy.

ACKNOWLEDGMENTS

The authors acknowledge the financial support from the Royal Norwegian Council for Scientific and Industrial Research. In addition, thanks are due to Dr. S.J. Andersen, Sintef Applied Physics, for valuable assistance during the course of the work.

REFERENCES

1. D.J. Abson, R.E. Dolby, and P.H.M. Hart: *Proc. Int. Conf. on Trends in Steel and Consumables for Welding*, London, 1978, The Welding Institute, Abington, Cambridge, 1978, pp. 75-101.
2. R.A. Ricks, P.R. Howell, and G.S. Barrite: *J. Mater. Sci.*, 1982, vol. 17, pp. 732-40.
3. R.C. Cochrane: *Weld. World*, 1983, vol. 21, pp. 21-24.
4. S. Liu and D.L. Olson: *Weld J.*, 1986, vol. 65, pp. 139s-150s.
5. Ø. Grong and D.K. Matlock: *Int. Met. Rev.*, 1986, vol. 31, pp. 27-48.
6. D.J. Abson and R.J. Pargeter: *Int. Met. Rev.*, vol. 31, pp. 141-94.
7. A.R. Mills, G. Thewlis, and J.A. Whiteman: *Mater. Sci. Technol.*, 1987, vol. 3, pp. 1051-62.
8. P.L. Harrison and R.A. Farrar: *Int. Mater. Rev.*, 1989, vol. 34, pp. 35-51.
9. M. Strangwood and H.K.D.H. Bhadeshia: *Proc. Int. Conf. on Advances in Welding Science and Technology*, Gatlinburg, TN, 1986, ASM INTERNATIONAL, Metals Park, OH, 1986, pp. 209-13.
10. A.O. Kluken, Ø. Grong, and J. Hjelen: *Metall. Trans. A*, 1991, vol. 22A, pp. 657-63.

11. J.R. Yang and H.K.D.H. Bhadeshia: *Mater. Sci. Technol.*, 1989, vol. 5, pp. 93-97.
12. J.M. Dowling, J.M. Corbett, and H.W. Kerr: *Metall. Trans. A*, 1986, vol. 17A, pp. 1611-23.
13. A.O. Kluken and Ø. Grong: *Metall. Trans. A*, 1989, vol. 20A, pp. 1335-49.
14. A.O. Kluken, Ø. Grong, and G. Rørvik: *Metall. Trans. A*, 1990, vol. 21A, pp. 2047-58.
15. S.P. Ringer, W.B. Li, and K.E. Easterling: *Acta Metall. Mater.*, 1992, vol. 40, pp. 275-83.
16. S. Liu: in *Ferrous Alloy Weldments*, D.L. Olson and T.H. North, eds., Trans Tech Publications, Zürich, 1992, pp. 1-18.
17. Ø. Grong and A.O. Kluken: in *Ferrous Alloy Weldments*, D.L. Olson and T.H. North, eds., Trans Tech Publications, Zürich, 1992, pp. 21-46.
18. L. Devillers, D. Kaplan, B. Marandet, A. Ribes, and P.V. Ribound: *Proc. Int. Conf. on Effects of Residual, Impurity and Alloying Elements on Weldability and Weld Properties*, London, Nov. 1983, Paper 1, The Welding Institute, Abington, Cambridge, 1983.
19. C. Bonnet and F.P. Charpentier: *Proc. Int. Conf. on Effects of Residual, Impurity and Alloying Elements on Weldability and Weld Properties*, London, Nov. 1983, Paper 8, The Welding Institute, Abington, Cambridge, 1983.
20. M.E. Saggese, D.N. Hawkins, and J.A. Whiteman: *Proc. Int. Conf. on Effects of Residual, Impurity and Alloying Elements on Weldability and Weld Properties*, London, Nov. 1983, Paper 15, The Welding Institute, Abington, Cambridge, 1983.
21. R.A. Farrar and P.L. Harrison: *J. Mater Sci.*, 1987, vol. 22, pp. 3812-20.
22. G.M. Evans: *Weld. J.*, 1992, vol. 71, pp. 447s-454s.
23. M. Es-Souni, P.A. Beaven, and G.M. Evans: *Mater. Sci. Eng.*, 1990, vol. A130, pp. 173-84.
24. S. Liu and D.L. Olson: *J. Mater. Eng.*, 1987, vol. 9, pp. 237-51.
25. S. Liu: Ph.D. Thesis, Colorado School of Mines, Golden, CO, 1984.
26. P.E. Marth, H.I. Aaronson, G.W. Lorimer, T.L. Bartel, and K.C. Russell: *Metall. Trans. A*, 1976, vol. 7A, pp. 1519-28.
27. H.K.D.H. Bhadeshia and L.E. Svensson: in *Mathematical Modelling of Weld Phenomena*, H. Cerjack and K.E. Easterling, eds., The Institute of Materials, London, 1993, pp. 109-80.
28. P.L. Ryder, W. Pitsch, and R.F. Mehl: *Acta Metall.*, 1967, vol. 15, pp. 1431-40.
29. F.J. Barbaro, P. Krauklis, and K.E. Easterling: *Mater. Sci. Technol.*, 1989, vol. 5, pp. 1057-68.
30. W.C. Johnson, C.L. White, P.E. Marth, P.K. Ruf, S.M. Tuominen, K.D. Wade, K.C. Russell, and H.I. Aaronson: *Metall. Trans. A*, 1975, vol. 6A, pp. 911-19.
31. H. Terashima and P.H.M. Hart: Technical Report No. 186, The Welding Institute, Abington, Cambridge, 1982.
32. A.O. Kluken and Ø. Grong: Technical Report No. STF34 A87001, SINTEF, Trondheim, Norway, 1986.